Cascade of Solitonic Excitations in a Superfluid Fermi gas: From Planar Solitons to Vortex Rings and Lines

Mark J. H. Ku, Biswaroop Mukherjee, Tarik Yefsah, and Martin W. Zwierlein
MIT-Harvard Center for Ultracold Atoms, Research Laboratory of Electronics, and Department of Physics, Massachusetts Institute of Technology, Cambridge, Massachusetts 02139, USA
(Received 5 July 2015; published 27 January 2016)

We follow the time evolution of a superfluid Fermi gas of resonantly interacting ^{6}Li atoms after a phase imprint. Via tomographic imaging, we observe the formation of a planar dark soliton, its subsequent snaking, and its decay into a vortex ring, which, in turn, breaks to finally leave behind a single solitonic vortex. In intermediate stages, we find evidence for an exotic structure resembling the Φ soliton, a combination of a vortex ring and a vortex line. Direct imaging of the nodal surface reveals its undulation dynamics and its decay via the puncture of the initial soliton plane. The observed evolution of the nodal surface represents dynamics beyond superfluid hydrodynamics, calling for a microscopic description of unitary fermionic superfluids out of equilibrium.

DOI: 10.1103/PhysRevLett.116.045304

Solitonic excitations such as solitons, vortices, and vortex rings are found in a large variety of nonlinear media, from classical fluids and plasmas to polyacetylene chains and superconductors. While ubiquitous, their intrinsic properties are tailored by the host medium. In superfluids, which are characterized by a complex order parameter with a well-defined phase and a nonviscous flow, such excitations correspond to phase defects and exhibit properties nonexistent in their classical counterparts. In particular, a vortex is topologically protected owing to the quantized circulation of the velocity field, and a traveling soliton experiences superfluid back flow determined by the phase difference across it [1,2]. The quantum statistics of the particles forming the superfluid is yet another ingredient which dramatically affects the properties of these defects. In Fermi superfluids, as opposed to the bosonic case, dark solitons and vortices are known to host in-gap fermionic excitations in their cores, from the Andreev bound states in the generic case [3,4], to the more exotic Majorana fermions in the presence of spin-orbit coupling [5,6].

Importantly, in a quantum fluid with short-ranged interactions, these phase defects are localized within the microscopic length scale of the system: the healing length ξ. The healing length sets the length scale above which the superfluid dynamics is well captured by the hydrodynamic formalism. At length scales on the order of ξ or smaller, a microscopic description is required, and this is where the dichotomy between Bose superfluids and Fermi superfluids becomes stringent. While weakly interacting Bose-Einstein condensates (BECs) are well understood in terms of the Gross-Pitaevskii (GP) theory, a complete microscopic wave equation for strongly interacting Fermi superfluids remains to be established. At the mean-field level, a unified description can be formulated within the Bogoliubov–de Gennes (BDG) formalism, which connects to the GP equation in the limit of weakly interacting BECs, and contains the necessary fermionic degrees of freedom in the Bardeen-Cooper-Schrieffer (BCS) limit [1,2,4,7]. However, while the BDG framework provides a good description of these two limiting cases, it is unclear whether it contains the right ingredients to quantitatively handle the short-range behavior of solitonic excitations in the strongly correlated regime [8]. The unitary Fermi gas realized in ultracold atom experiments offers a unique opportunity to clarify this issue, as it resides at the point of the BEC-BCS crossover where beyond mean-field correlations are expected to be the strongest [9]. It is also the regime where the healing length ξ is the smallest—on the order of the interparticle spacing—such that phase defects are as localized as possible in a quantum fluid.

A natural approach to experimentally revealing the core dynamics of such defects is to trigger their decay. Solitonic excitations, indeed, follow a well-defined hierarchy in terms of stability and energy cost in three dimensions, the planar soliton being the most energetic and unstable towards the formation of other solitary waves [10–15]. In weakly interacting BECs, dark solitons have been observed decaying into vortex rings and vortices [16–20] as a consequence of the snake instability, the undulation of the soliton plane [10]. In the case of strongly interacting Fermi superfluids, similar scenarios have been predicted numerically within a mean-field approximation [21–23], but an experimental support of such microscopic dynamics is still lacking.

In this Letter, we create a cascade of solitonic excitations in a unitary Fermi gas of ^{6}Li atoms. Starting from a planar dark soliton created via phase imprinting, we observe the formation of ring defects which eventually decay into a single solitonic vortex. By means of a tomographic imaging

 © 2016 American Physical Society

technique [24], we are able to follow the surface dynamics of the soliton's nodal plane at the level of the interparticle spacing, as it snakes, breaks, and converts into the topologically protected solitonic vortex. Our measurements allow for a quantitative analysis of the snaking dynamics of the initial dark soliton, awaiting comparison to time-dependent theories of strongly correlated fermions.

We create a strongly interacting fermionic superfluid using a balanced mixture of the two lowest hyperfine states of ^{6}Li ($|1\rangle$ and $|2\rangle$) at a Feshbach resonance [25]. Our atomic clouds contain $\sim 7 \times 10^5$ atoms per spin state confined in an elongated trap, combining a radial optical potential in the x-y plane [trapping frequency $\omega_\perp/2\pi = 69(6)$ Hz] and a shallower axial magnetic potential along the z axis [trapping frequency $\omega_z/2\pi = 10.87(1)$ Hz]. The axial and radial Thomas-Fermi radii of the cloud are $R_z = 326$ μm and $R_\perp = 54$ μm, and correspond to a chemical potential at the center of the cloud $\mu = h \times 3.7(2)$ kHz $= 54(5)\hbar\omega_\perp$. The gas is, thus, deep in the three-dimensional regime. Gravity slightly weakens the trapping potential along the vertical y direction [26]. Phase imprinting is realized as in Refs. [24,28–31], whereby one half of the superfluid is exposed to a blue-detuned laser beam for a time sufficient to advance the phase by approximately π. These experimental parameters are similar to those of previous works [24,31], where a single solitonic vortex was detected and observed to undergo a deterministic precessional motion for several seconds. Here, we study the evolution of the excitations at early times following the phase imprint. To probe such dynamics, we combine the so-called rapid ramp technique and tomographic imaging [24,26]. In our experimental sequence, the rapid ramp is performed at a variable wait time t following the imprint. We then slice a thin layer of the atomic cloud at a chosen y position, and destructively probe its density distribution via absorption imaging.

Figure 1(a) shows a time sequence of images recorded in the first 20 ms after the phase imprint, which corresponds to the density distribution at the central slice (near $y = 0$) of the superfluid. At the location of the imprinted phase jump ($z = 0$), a slow and straight dark soliton emerges and, subsequently, undergoes a snaking motion, seeding the puncture of the nodal surface. The broken soliton evolves into a ring structure, visible in the central slice as a pair of nodal points. Figure 1(b) presents a zoomed-in view of the soliton's time evolution up to 100 ms after the imprint. Simultaneous with the soliton's core dynamics, two wave fronts quickly propagate to the edges of the cloud, which we identify as sound waves. The upper and lower sound wave fronts are found to propagate at speeds of 13.1(4) mm/s and 13.1(8) mm/s, respectively, which coincide with the speed of sound of 12.9(1) mm/s estimated from the peak density using the relation $c_s = \sqrt{\xi_B/3}v_F$, where $\xi_B = 0.37$ is the Bertsch parameter [32] and v_F the Fermi velocity. The apparent large amplitude of these sound waves is a consequence of the rapid ramp [26].

The dynamics is analyzed in detail in Fig. 2, showing residuals of the central slice as a function of time, along the axial cut at $x = 0$ [Fig. 2(b)] and along its outer edge near $x = R_\perp$ [Fig. 2(c)]. The difference between the characteristic speeds of the various waves generated after the phase imprint is striking. One recognizes the two initially created sound waves following linear trajectories with opposite slopes, while the dark soliton remains near $z = 0$ with negligible velocity. A second set of shallower sound waves is emitted about $\sim$5 ms after the initial sound wave fronts, forming all together a pattern of hydrodynamic wakes. The rapid vanishing of the sound contrasts with the persistence of the solitonic wave near $z = 0$. Close to 100 ms after the imprint, a single solitonic vortex remains, precessing in the

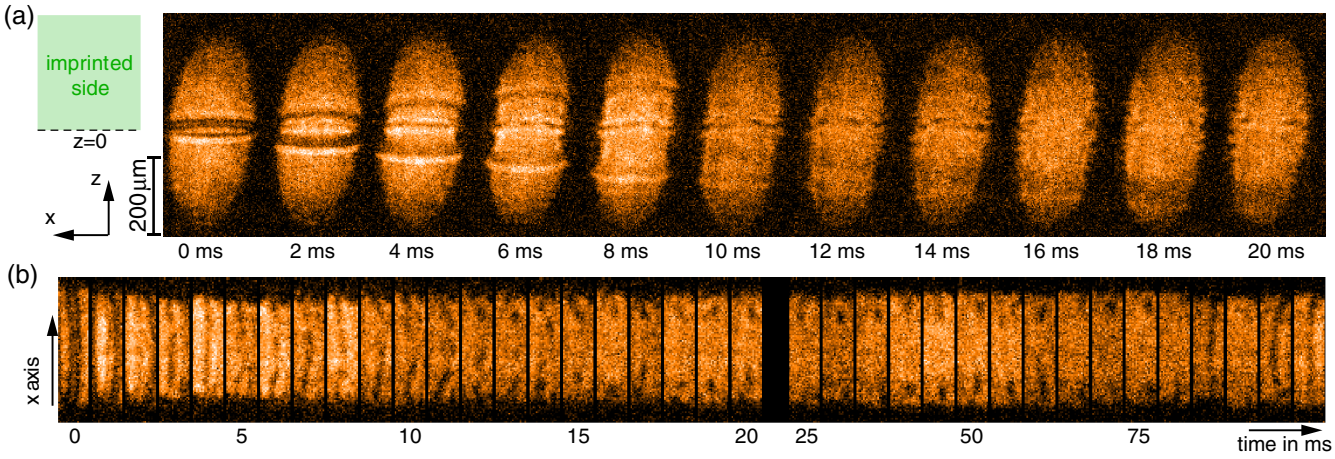

FIG. 1. (a) Cascade of solitonic excitations in a unitary Fermi superfluid following the phase imprint. A planar soliton snakes and decays into a vortex ring. Shown are images of the density distribution in the central slice of the superfluid, after rapid ramp and time of flight, for the first 20 ms after the imprint. The imprint also generates two sound waves propagating towards the edges. (b) Time series of the central slice up to $t = 100$ ms, cropped to the region around $z = 0$.

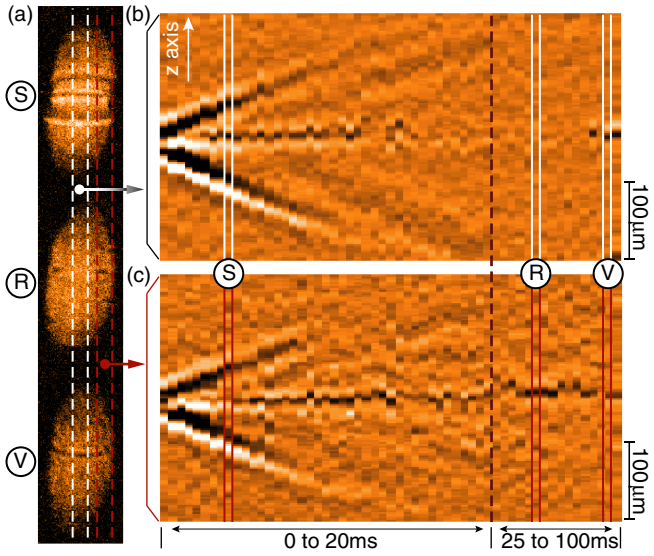

FIG. 2. Overview of the dynamics following the phase imprinting. (a) Representative images of the central slice at $t = 4$, 50, and 95 ms showing a planar soliton (S), the nodal points of a vortex ring (R), and a vortex line (V). The vertical lines indicate the regions of interest for the generation of residuals in (b) and (c). (b,c) Residuals on the central slice along the central axial cut $x = 0$ (b) and an outer axial cut (c). Dark (bright) color indicates density depletion (excess). Two sound waves rapidly propagate to the edges, while a sharp depletion remains at the center. Around $t = 5$ ms, a second set of shallower sound waves is emitted. The residuals show the puncture of the soliton plane in the central slice ($t \sim 15$ ms) and the return of a vortex line at $t \sim 80$ ms.

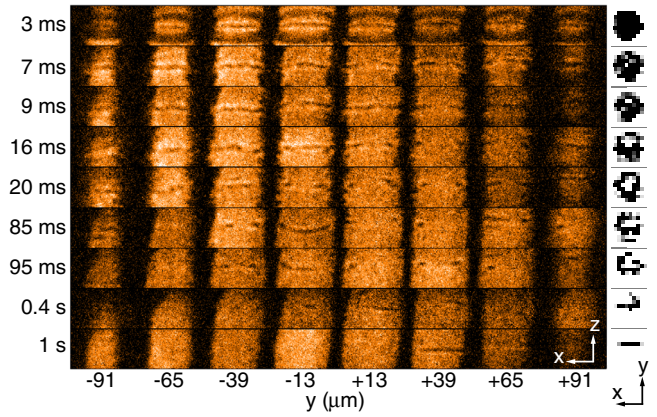

FIG. 3. Tomography of the cascade. Main panel (left): representative tomographic images at different stages of the cascade. The field of view is centered on the defect's z position. Right column: structure of the depletion due to the defect, as would be seen along the z axis, reconstructed from the tomographic images. $t = 3$ ms: sharp density depletion across the whole cloud signaling a planar dark soliton. $t = 7$ ms: snaking of the soliton plane and first signature of a puncture. $t = 9$, 16, and 20 ms: the puncture in the upper half of the soliton plane grows and yields an asymmetric vortex ring, with a nodal area left at the bottom. $t = 85$ ms: the lower nodal area is punctured and a vortex line forms across a vortex ring. $t = 95$ and 400 ms: the ring part of the defect progressively disintegrates. $t = 1000$ ms: a single solitonic vortex remains.

superfluid, with a period of $\sim$1.4 s along the z axis [24,26,31], which is more than an order of magnitude longer than the duration of the cascade.

In order to obtain a complete picture of the dynamics, three-dimensional tomography of the superfluid is performed. Figure 3 displays a set of representative tomographic images at various times, giving access to the local pair density after the rapid ramp. From these images, we are able to reconstruct the structure of the defect engraved in the superfluid and follow its time evolution. The right panel of Fig. 3 shows the reconstructed depletion as would be seen from the long axis of the cloud. At early times, a surface of depletion cutting through the entire cloud's section is observed: the planar dark soliton. It, subsequently, tears in its upper half and then undergoes a cascade into structures with smaller and smaller nodal area. The hole appearing in the initial nodal surface is seen to continuously grow in size, leading to the formation of a transient asymmetric vortex ring, combining the bottom part of the initial soliton and a vortex line bent in a semicircle on the upper part. At this stage, one might anticipate that the nodal area will naturally heal into a standard vortex ring by shrinking into a single loop with a core of size ξ. However, the tomographic images obtained at later times suggest a more complicated scenario [26], where a second puncture occurs in the lower nodal plane. This results in the formation of a horizontal line depletion which we interpret as a vortex line intersecting the vortex ring. This structure is seen in the tomographic images, e.g., at $t = 85$ ms in Fig. 3, and it resembles the Φ soliton recently proposed in Ref. [15]. At even later times, the ring part of this exotic defect progressively disintegrates (as seen at $t = 95$ ms and 400 ms in Fig. 3), leaving behind a single solitonic vortex ($t = 1$ s), which precesses in the superfluid. It is the precession of this remnant solitonic vortex which has been studied in [24,31].

Recently, several theoretical works have treated the evolution of fermionic superfluids following a phase imprint [21,23,33,34] and the possible cascade scenarios following the decay of a planar dark soliton [22,23,35,36] via various mean-field approaches. In some of these works, it has been numerically found that, in a cylindrically symmetric potential with negligible dissipation, a planar soliton decays into a vortex ring, which then undergoes a long-lived oscillatory motion along the z axis [22,35,36]. By mimicking experimental imperfections, such as trap distortions [21], and imperfect phase imprinting [23,34], later works found that the vortex ring further decays into a single remnant vortex. The proposed scenarios are, however, distinct from our observations. Recent simulations based on the GP equation reveal a variety of dynamical

pathways towards the final single vortex, via intermediate "Chladni solitons" [15,37].

At the origin of the cascade lies the snaking instability of the soliton. In order to quantify this undulation dynamics, we perform a Fourier analysis on the soliton's shape $z_s(x) \approx A_0 + \Sigma_{n=1}^{N} A_n \cos[2\pi n(x/2R_\perp) + \phi_n]$ in terms of the transverse modes of wavelengths $\lambda_n = 2R_\perp/n$, the integer n being the mode number, with Fourier amplitudes A_n and phases ϕ_n. Figure 4(a) displays selected images of the snaking soliton, and Fig. 4(b) the corresponding nodal profiles $z_s(x)$ obtained from the density minima. For each profile, the result of the Fourier expansion up to the fifth order (gold solid line) is superimposed, illustrating that the undulation observed here is well characterized in terms of transverse mode excitations. Fourier spectra of the soliton's undulation are obtained for $2\ \text{ms} \le t \le 11\ \text{ms}$ [see Fig. 4(c)], and the evolution of the amplitudes A_n is reported in Fig. 4(d). We find that the fundamental mode $\lambda_1 = 2R_\perp$ largely dominates this dynamics, with a relative weight consistently higher than that of the harmonics and a significantly larger growth velocity $\dot{A}_1$. The velocities $\dot{A}_n$ decrease as the mode number n increases [see Fig. 4(e)].

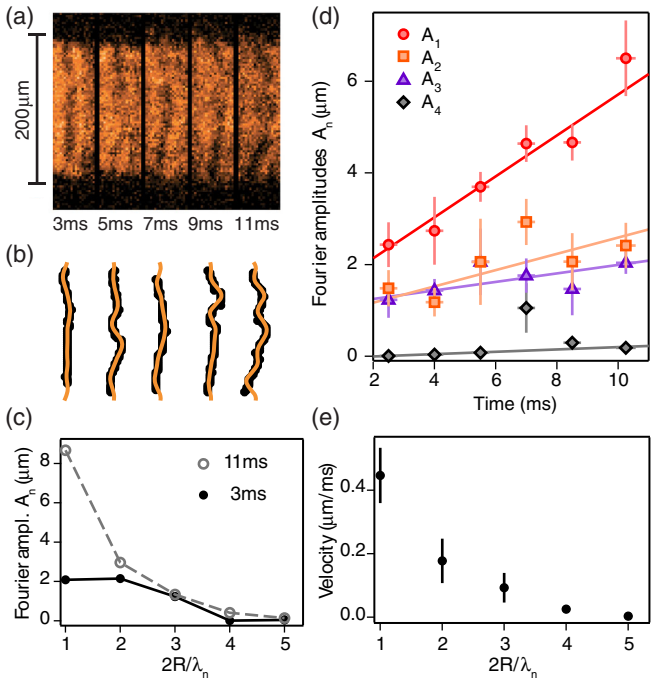

FIG. 4. Spectral analysis of the snaking dynamics. (a) Snapshots of the soliton's undulation (central slice at $y = -13\ \mu$m). (b) Extracted undulation shapes $z_s(x)$ (black dots) along with the corresponding Fourier expansions to the fifth order (solid gold line). (c) Fourier spectra at $t = 3$ and 11 ms. (d) Fourier amplitudes A_n as a function of time, for $n = 1$ (circle), 2 (square), 3 (triangle), and 4 (diamond) and their fits to a line (solid lines). The error bars indicate the standard deviation of the mean obtained from a three-point binning of the data. (e) Growth velocities $\dot{A}_n$ for $n = 1$ to 5, obtained from the linear fits in (d), with the error bars being the fit error.

The contribution of the modes $n > 5$ was found to be insignificant. Note that it is conceivable that the rapid ramp reduces the visibility of the modes $n \gtrsim 10$ as their wavelengths are on the order of the observed soliton width ($\sim 20\ \mu$m) or smaller.

Superfluid hydrodynamics predicts an exponential growth $A_n(t) = A_n(0)\exp(t/\tau_n)$ of each mode [38,39]. The linear growth observed here might reflect the early time dynamics $A_n(t) \approx A_n(0)(1 + t/\tau_n)$. For the fundamental mode, one finds a rate $\tau_1^{-1} = \dot{A}_1/A_1(0) \approx 2\pi \times 76$ Hz, close to the radial trapping frequency $\omega_\perp$. This is consistent with the result $\tau_1^{-1} = \omega_\perp$ of a stability analysis of solitons in a trapped superfluid [40]. However, the growth appears to remain linear, instead of exponential, for times $t > \tau_1$, which effect is possibly tied to the inhomogeneity of the transverse confinement. Indeed, within the local density approximation, each surface element of the soliton propagates at a fixed fraction of the local speed of sound, set by the current-phase relation [41,42]. This causes the bending of the soliton into a drumlike profile, whose amplitude increases at constant velocity. Further insight could be obtained by comparing the measured velocities $\dot{A}_n$ to results from numerical simulations along the lines of Ref. [39], with the inclusion of a transverse harmonic confinement.

In conclusion, we have observed a cascade of solitonic excitations in a strongly interacting Fermi superfluid, from an initial planar dark soliton towards a final, remnant solitonic vortex, through an intermediate ring structure resembling the recently predicted Φ soliton [15]. At the origin of the cascade lies the snaking instability, which we characterized quantitatively by studying the evolution of transverse Fourier modes. The breaking dynamics of the unitary Fermi gas studied here occurs at the scale of the interparticle spacing, and provides a novel experimental input for microscopic theories of strongly interacting fermions. A natural extension of our work is to approach a regime where the snake instability is inhibited, e.g., via a strong confining potential in the radial direction. Future prospects are a measurement of the soliton's current-phase relation in the BEC-BCS crossover [41,42], the detection and manipulation of Andreev bound states trapped inside the soliton [3,4], and the creation of soliton trains in the presence of spin imbalance, which would realize one limit of Fulde-Ferrell-Larkin-Ovchinnikov states [43–45].

We would like to thank Joachim Brand and Lev Pitaevskii for fruitful discussions, Julian Struck for a critical reading of the manuscript, and Parth Patel and Zhenjie Yan for assistance in the data analysis. This work was supported by the NSF, the ARO MURI on Atomtronics, AFOSR PECASE and MURI on Exotic Phases, and the David and Lucile Packard Foundation.

[1] R. G. Scott, F. Dalfovo, L. P. Pitaevskii, and S. Stringari, Phys. Rev. Lett. **106**, 185301 (2011).

[2] D. K. Efimkin and V. Galitski, Phys. Rev. A **91**, 023616 (2015).
[3] C. Caroli, P. d. Gennes, and J. Matricon, Phys. Lett. **9**, 307 (1964).
[4] M. Antezza, F. Dalfovo, L. P. Pitaevskii, and S. Stringari, Phys. Rev. A **76**, 043610 (2007).
[5] Y. Xu, L. Mao, B. Wu, and C. Zhang, Phys. Rev. Lett. **113**, 130404 (2014).
[6] X.-J. Liu, Phys. Rev. A **91**, 023610 (2015).
[7] W. Wen and G. Huang, Phys. Rev. A **79**, 023605 (2009).
[8] A. Bulgac and M. M. Forbes, *Quantum Gases: Finite Temperature and Non-Equilibrium Dynamics*, edited by M. D. N. P. Proukakis, S. A. Gardiner, and M. Szymanska, Cold Atoms Series Vol. 1 (Imperial College Press, London, 2013).
[9] *The BCS-BEC Crossover and the Unitary Fermi Gas*, edited by W. Zwerger (Springer, New York, 2011), Vol. 836.
[10] A. E. Muryshev, H. B. van Linden van den Heuvell, and G. V. Shlyapnikov, Phys. Rev. A **60**, R2665 (1999).
[11] D. L. Feder, M. S. Pindzola, L. A. Collins, B. I. Schneider, and C. W. Clark, Phys. Rev. A **62**, 053606 (2000).
[12] J. Brand and W. Reinhardt, J. Phys. B **34**, L113 (2001).
[13] J. Brand and W. P. Reinhardt, Phys. Rev. A **65**, 043612 (2002).
[14] S. Komineas and N. Papanicolaou, Phys. Rev. A **68**, 043617 (2003).
[15] A. Muñoz Mateo and J. Brand, Phys. Rev. Lett. **113**, 255302 (2014).
[16] B. P. Anderson, P. C. Haljan, C. A. Regal, D. L. Feder, L. A. Collins, C. W. Clark, and E. A. Cornell, Phys. Rev. Lett. **86**, 2926 (2001).
[17] Z. Dutton, M. Budde, C. Slowe, and L. V. Hau, Science **293**, 663 (2001).
[18] I. Shomroni, E. Lahoud, S. Levy, and J. Steinhauer, Nat. Phys. **5**, 193 (2009).
[19] C. Becker, K. Sengstock, P. Schmelcher, P. G. Kevrekidis, and R. Carretero-Gonzlez, New J. Phys. **15**, 113028 (2013).
[20] S. Donadello, S. Serafini, M. Tylutki, L. P. Pitaevskii, F. Dalfovo, G. Lamporesi, and G. Ferrari, Phys. Rev. Lett. **113**, 065302 (2014).
[21] G. Wlazłowski, A. Bulgac, Michael McNeil Forbes, and K. J. Roche, Phys. Rev. A **91**, 031602 (2015).
[22] M. D. Reichl and E. J. Mueller, Phys. Rev. A **88**, 053626 (2013).
[23] P. Scherpelz, K. Padavic, A. Rancon, A. Glatz, I. S. Aranson, and K. Levin, Phys. Rev. Lett. **113**, 125301 (2014).
[24] M. J.-H. Ku, W. Ji, B. Mukherjee, E. Guardado-Sanchez, L. W. Cheuk, T. Yefsah, and M. W. Zwierlein, Phys. Rev. Lett. **113**, 065301 (2014).
[25] W. Ketterle and M. Zwierlein, Riv. Nuovo Cimento Soc. Ital. Fis. **31**, 247 (2008).
[26] See Supplemental Material at http://link.aps.org/supplemental/10.1103/PhysRevLett.116.045304 for further details on experimental parameters and procedures, data analysis and additional data, which includes Ref. [27].
[27] M. W. Zwierlein, J. R. Abo-Shaeer, A. Schirotzek, C. H. Schunck, and W. Ketterle, Nature (London) **435**, 1047 (2005).
[28] S. Burger, K. Bongs, S. Dettmer, W. Ertmer, K. Sengstock, A. Sanpera, G. V. Shlyapnikov, and M. Lewenstein, Phys. Rev. Lett. **83**, 5198 (1999).
[29] J. Denschlag, J. E. Simsarian, D. L. Feder, C. W. Clark, L. A. Collins, J. Cubizolles, L. Deng, E. W. Hagley, K. Helmerson, W. P. Reinhardt, S. L. Rolston, B. I. Schneider, and W. D. Phillips, Science **287**, 97 (2000).
[30] C. Becker, S. Stellmer, P. Soltan-Panahi, S. Döscher, M. Baumert, E. M. Richter, J. Kronjäger, K. Bongs, and K. Sengstock, Nat. Phys. **4**, 496 (2008).
[31] T. Yefsah, A. T. Sommer, M. J. H. Ku, L. W. Cheuk, W. Ji, W. S. Bakr, and M. W. Zwierlein, Nature (London) **499**, 426 (2013).
[32] M. J. H. Ku, A. T. Sommer, L. W. Cheuk, and M. W. Zwierlein, Science **335**, 563 (2012).
[33] K. Sacha and D. Delande, Phys. Rev. A **90**, 021604 (2014).
[34] P. Scherpelz, K. Padavić, A. Murray, A. Glatz, I. S. Aranson, and K. Levin, Phys. Rev. A **91**, 033621 (2015).
[35] A. Bulgac, Michael McNeil Forbes, M. M. Kelley, K. J. Roche, and G. Wlazlowski, Phys. Rev. Lett. **112**, 025301 (2014).
[36] W. Wen, C. Zhao, and X. Ma, Phys. Rev. A **88**, 063621 (2013).
[37] J. Brand (private communication).
[38] A. M. Kamchatnov and L. P. Pitaevskii, Phys. Rev. Lett. **100**, 160402 (2008).
[39] A. Cetoli, J. Brand, R. G. Scott, F. Dalfovo, and L. P. Pitaevskii, Phys. Rev. A **88**, 043639 (2013).
[40] L. Pitaevskii (private communication).
[41] A. Spuntarelli, L. D. Carr, P. Pieri, and G. C. Strinati, New J. Phys. **13**, 035010 (2011).
[42] R. G. Scott, F. Dalfovo, L. P. Pitaevskii, S. Stringari, O. Fialko, R. Liao, and J. Brand, New J. Phys. **14**, 023044 (2012).
[43] N. Yoshida and S. K. Yip, Phys. Rev. A **75**, 063601 (2007).
[44] L. Radzihovsky, Phys. Rev. A **84**, 023611 (2011).
[45] R. M. Lutchyn, M. Dzero, and V. M. Yakovenko, Phys. Rev. A **84**, 033609 (2011).